Generating and measuring nondiffracting vector Bessel beams

Angela Dudley,[1] Yanming Li,[2] Thandeka Mhlanga,[1,3] Michael Escuti,[2] and Andrew Forbes[1,3,*]

[1]*CSIR National Laser Centre, P.O. Box 395, Pretoria 0001, South Africa*

[2]*Department of Electrical and Computer Engineering, North Carolina State University, Raleigh, North Carolina 27695, USA*

[3]*School of Physics, University of KwaZulu-Natal, Private Bag X54001, Durban 4000, South Africa*

**Corresponding author: AForbes1@csir.co.za*

Received June 26, 2013; revised August 1, 2013; accepted August 4, 2013;
posted August 7, 2013 (Doc. ID 192892); published August 29, 2013

Nondiffracting vector Bessel beams are of considerable interest due to their nondiffracting nature and unique high-numerical-aperture focusing properties. Here we demonstrate their creation by a simple procedure requiring only a spatial light modulator and an azimuthally varying birefringent plate, known as a *q*-plate. We extend our control of both the geometric and dynamic phases to perform a polarization and modal decomposition on the vector field. We study both single-charged Bessel beams as well as superpositions and find good agreement with theory. Since we are able to encode nondiffracting modes with circular polarizations possessing different orbital angular momenta, we suggest these modes will be of interest in optical trapping, microscopy, and optical communication. © 2013 Optical Society of America

OCIS codes: (140.3295) Laser beam characterization; (090.1995) Digital holography; (050.2770) Gratings; (050.4865) Optical vortices.

http://dx.doi.org/10.1364/OL.38.003429

There has been considerable interest of late in optical modes of spatially inhomogeneous polarization states, for example cylindrical symmetric polarization, commonly referred to as cylindrical vector (CV) beams [1–4] that includes radially and azimuthally polarized light, and a linear superposition of the two to form generalized cylindrical polarization. In the cross-sectional profile of these CV beams, the local polarization state is linearly polarized at different orientations, resulting in them occupying the equator on the Poincaré sphere. Recently a more general type of vector beam [full Poincaré (FP) beams] has been proposed and demonstrated [5,6] where the local polarization state spans the entire surface of the Poincaré sphere. Various generation methods of CV and FP beams have been developed from laser gain media [7,8], optical fibers [9], radial polarization converters [10,11], liquid crystal displays [12], *q*-plates [13], and interferometric methods [14]. CV beams exhibit unique properties under high numerical-aperture focusing giving rise to the realization of tighter focal spots [15–18] resulting in applications in spectroscopy, particle acceleration, microscopy, optical trapping, and interferometry [1–4]. These beams have interesting propagation characteristics: in free space due to the manifestation of the universal form of the Gouy phase of astigmatic wave fields [19] and have been shown to be more resilient to atmospheric turbulence [20].

It is also possible to generate such vector beams as vector–vortex beams. Scalar vortex fields carry orbital angular momentum (OAM) and have an azimuthal angular dependence of $\exp(i\ell\theta)$ where ℓ is the azimuthal index and θ is the azimuthal angle. One such example of propagation-invariant scalar modes which are OAM carriers are higher-order Bessel beams [21,22]. Experimental studies into the generation of diffraction-limited vector beams have remained somewhat limited with reports on the use of subwavelength gratings [23], polarization grating (PG) axicons [24], quantized Pancharatnam Berry phase elements in conjugation with an axicon [25], and interferometric techniques [26,27].

In this Letter, we present a new procedure for the generation and measurement of nondiffracting vector Bessel beams. We control both the dynamic and geometric phase, using a spatial light modulator (SLM) and *q*-plate, to convert arbitrary incoming scalar fields into nondiffracting vector fields. We simultaneously detect both the polarization and azimuthal components of our vector Bessel beam by implementing a PG in conjugation with a second SLM to perform a polarization selective azimuthal modal decomposition. Although this technique is outlined with Bessel beams as the spatial modes, it can easily be extended to other OAM-carrying modes.

We illustrate the concept for both the generation and measurement of vector Bessel beams with the aid of Fig. 1. To generate arbitrary superpositions of scalar Bessel beams an expanded HeNe laser beam ($\lambda \sim 633$ nm) was directed onto the first SLM (SLM1). These fields were generated in a similar approach to Durnin's ring-slit aperture method [21], implemented digitally [22] on SLM1 (HoloEye, PLUTO-VIS, with

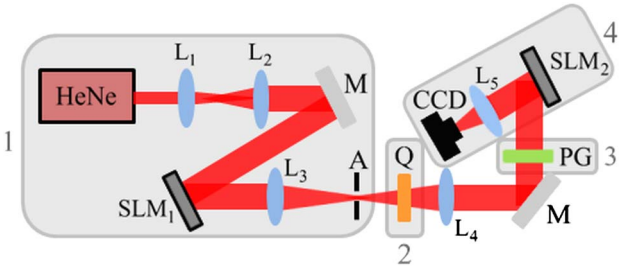

Fig. 1. Schematic of the experimental setup [division 1, scalar generation; division 2, vector generation; division 3, vector decomposition; division 4, scalar (azimuthal) decomposition]. L, lens ($f1 = 15$ mm, $f2 = 150$ mm, $f3$ and $f4 = 500$ mm, $f5 = 300$ mm); SLM, spatial light modulator; A, aperture; *Q*, *q*-plate; PG, polarization grating; CCD, camera.

1920×1080 pixels of pitch 8 μm and calibrated for a 2π phase shift at ~633 nm) with the use of complex amplitude modulation [28–30]. Mathematically we may describe such a generalized superposition of Bessel beams as

$$u(r,\phi,z=0) = \sum_{\ell} J_{\ell}(k_r r)\exp(i\ell\phi)\begin{pmatrix}1\\1\end{pmatrix}, \quad (1)$$

where $J_{\ell}(\cdot)$ is the Bessel function of the first kind, k_r is the transverse wave vector and the Jones vector denotes linear polarization. To convert this scalar field into a CV field, we introduce in the second step (2) an azimuthally varying birefringent plate, known as a q-plate, which couples OAM to spin angular momentum through the transformation

$$\begin{pmatrix}\cos(Q\phi) & \sin(Q\phi)\\ \sin(Q\phi) & -\cos(Q\phi)\end{pmatrix}\begin{pmatrix}1\\1\end{pmatrix}\exp(i\ell\phi)$$
$$\rightarrow \exp(i(\ell+Q)\phi)\begin{pmatrix}1\\-i\end{pmatrix} + \exp(i(\ell-Q)\phi)\begin{pmatrix}1\\i\end{pmatrix}, \quad (2)$$

where the first matrix corresponds to the Jones matrix for a q-plate [31] and Q is the azimuthal charge introduced by the q-plate ($Q = 2q$). The two vectors correspond to right- and left-circular polarization, respectively. The action of the q-plate [given by the Jones matrix in Eq. (2)] can be represented in bra–ket notation as follows: $|\ell, L\rangle \rightarrow |\ell + Q, R\rangle$ and $|\ell, R\rangle \rightarrow |\ell - Q, L\rangle$, where R and L represent right- and left-circular polarization, respectively. The q-plate was manufactured as a polymerizable liquid crystal film on a glass substrate, whose spatial variation of the optical axis was realized by photoaligning the local director of the liquid crystalline material with UV light [32,33]. The UV light was shaped to a narrow stripe which was exposed onto the sample azimuthally with a rotating linear polarization. The concept of this coupling of angular momenta is shown in Fig. 2(a), where an experimentally generated circularly polarized Gaussian beam is converted into an oppositely handed vortex beam. The optical field after the q-plate ($Q = 1$) was therefore a vector Bessel beam described by $u \propto |\ell + 1, R\rangle + |\ell - 1, L\rangle = \exp(i\ell\phi)[|1, R\rangle + |-1, L\rangle]$, which we note is a radial polarized state since

$$|1,R\rangle + |-1,L\rangle = \exp(i\phi)\begin{pmatrix}1\\-i\end{pmatrix} + \exp(-i\phi)\begin{pmatrix}1\\i\end{pmatrix}$$
$$= \begin{pmatrix}\cos(\phi)\\ \sin(\phi)\end{pmatrix}. \quad (3)$$

To perform a modal decomposition on the vector vortex beam we again exploit both the dynamic and geometric phases. We employ a PG with a period of 8.3 μm, which acts as a polarizing beam splitter for left- and right-circular polarization, to split the field into its two spin components (step 3 in Fig. 1), and also shown in Fig. 2(b). The process for manufacturing the PG is similar to that for the q-plate; however, a polarization holography setup was used where the sample was exposed with the interference of two plane waves each of opposite circular polarization [33,34]. With the vector beam projected into two path-dependent scalar beams, we finally perform a modal decomposition on each to reconstruct the full vector vortex beam. We consider the modal decomposition of our input field E into azimuthal modes $\exp(i\ell\phi)$ so that $E = \sum_{\ell} c_{\ell} \exp(i\ell\phi)$. The modal weighting coefficients c_{ℓ} may be found by the inner product of the field with an azimuthal match filter, $|\langle E|\exp(i\ell\phi)\rangle| = c_{\ell}$. The inner product was executed experimentally by directing the modes onto the match filter, encoded on SLM2 and viewing the Fourier transform, with the use of lens L3, on the CCD (Spiricon BeamGage, SP620U). SLM2 is also only responsive to horizontally polarized modes. However, since the horizontal component is present in both left- and right-circular polarizations, we need not introduce additional polarization optics. The PG was aligned appropriately so that the port containing the left-circular polarization modes were incident on SLM2 so as to extract their azimuthal modes. Later, the PG was adjusted to direct the right-circular polarization modes onto SLM2 for the execution of their azimuthal decomposition. We point out that this could be done in a single step by directing both components to adjacent sectors of SLM2.

Scalar Bessel beams as well as superpositions thereof were created with SLM1, with near- and far-field images shown in the top row of Fig. 3. Figure 3(a) shows a

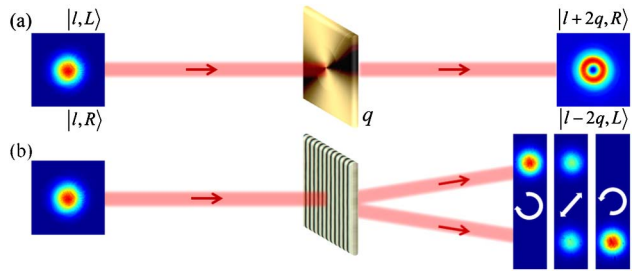

Fig. 2. (a) Transform of a q-plate with corresponding state equations. (b) The action of a PG with the incoming polarization marked in the corresponding outputs.

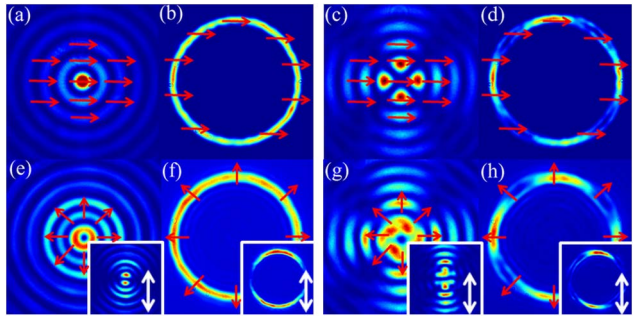

Fig. 3. Experimentally recorded near- and far-field intensity profiles of (a) and (b) the scalar single-charged Bessel beam of azimuthal index $\ell = 0$; (c) and (d) superposition of azimuthal indices $\ell = -2$ and $+2$. (e)–(h) Experimental near-field [(e) and (g)] and far-field [(f) and (h)] intensity profiles of the corresponding vector Bessel fields recorded after the q-plate. Insets denote the corresponding vector beams recorded with a polarizer in front of the CCD. Red (white) arrows denote the polarization direction (polarizer orientation).

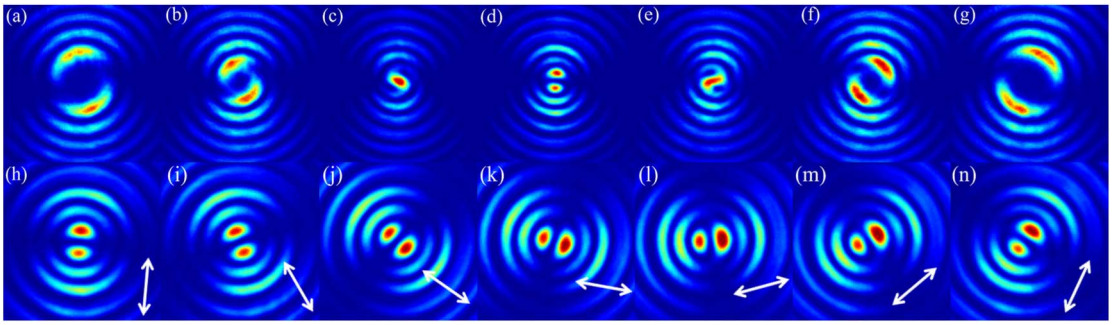

Fig. 4. (a)–(g) Experimentally recorded near-field intensity profiles of vector Bessel fields recorded after the q-plate with a polarizer in front of the CCD for initial scalar Bessel beams of $\ell = -5, -3, -1, 0, +1, +3$, and $+5$, respectively. (h)–(n) Intensity profiles for an $\ell = 0$ vector Bessel beam recorded with a rotating polarizer. The full data (video) can be viewed in Media 1. White arrows mark the corresponding polarizer setting.

zero-order Bessel beam recorded at the aperture (A) in Fig. 1 and its corresponding far-field depicted in Fig. 3(b), and similarly in Figs. 3(c) and 3(d) for a superposition of Bessel beams of azimuthal indices $\ell = -2$ and $+2$. In the case of the superposition, the azimuthal indices are of equal magnitude but opposite handedness resulting in the predicted petal structure, where the number of petals is denoted by $2|\ell|$ [22]. The fields entering the q-plate are linearly polarized (an equal weighting of left- and right-circular polarization) and so the transformation of Eq. (2) takes place: the left-circular component is converted to the right-circular component, while decreasing the azimuthal component by unit charge of OAM while the reserve procedure takes place on the right-circular component, converting it to left while simultaneously increasing the azimuthal component by unit charge of OAM ($|\ell, L\rangle \rightarrow |\ell + Q, R\rangle$ and $|\ell, R\rangle \rightarrow |\ell - Q, L\rangle$). The resulting field after the q-plate, is shown in Figs. 3(e) and 3(g). These are nondiffracting vector Bessel beams with radial polarization, as described by Eq. (3). In the case of the zero-order Bessel beam, the OAM associated with the left-circular component increases by unit charge of OAM (while the right-circular component decreases by unit charge of OAM), thus producing a superposition of two Bessel beams of azimuthal indices $\ell = -1$ and $+1$, resulting in an intensity structure with two petals ($2|\ell|$) as seen through a polarizer and shown in the insert in Fig. 3(e). Similarly, the superimposed Bessel beams of azimuthal indices $\ell = -2$ and $+2$ becomes a superimposition of Bessel beams of azimuthal indices $\ell = -3, -1, +1$, and $+3$ after the q-plate, as illustrated in Fig. 3(g). The corresponding far fields of Figs. 3(e) and 3(g) are given in Figs. 3(f) and 3(h). Here the number of line singularities in the far field is denoted by $2|\ell|$ (the same as the number of petals), as illustrated in the inserts in Figs. 3(f) and 3(h). While the aforementioned examples illustrate the technique, there is of course a myriad of choices for which vector Bessel beams to create. We show in Figs. 4(a)–4(g) additional experimental near-field images of vector Bessel fields (with a polarizer) for initial scalar beams of azimuthal indices ranging from $\ell = -5$ to $\ell = +5$. A polarizer (positioned after the q-plate) was rotated to illustrate that the intensity profile of the vector Bessel field rotates. Snapshots of the intensity profiles for a CV Bessel beam (for an initial single scalar Bessel beam of $\ell = 0$) is presented in Figs. 4(h)–4(n), illustrating the rotation of the field as the polarizer is rotated.

An azimuthal decomposition [35,36] was performed digitally on each polarization component of the generated fields and the results are depicted in Fig. 5(a) for the left- (orange) and right-circular (pink) components, respectively. The measurement of the azimuthal indices, presented in Fig. 5(a) (orange) [Fig. 5(a) (pink)], illustrates that the scalar single-charged Bessel beams incur an increase (decrease) in their OAM when passing through the q-plate, as expected from the transformation in Eq. (2). This is evident by the two rows of off-diagonal peaks, displaced from the original by ± 1. Figures 5(b) and 5(c) denote the left- and right-circular components (of azimuthal indices $\ell = +1$ and $\ell = -1$, respectively), which make up the vector vortex beam presented in Fig. 3(e).

In conclusion, we have shown an experimental realization of nondiffracting vector Bessel beams through control of both the dynamic and geometric phase. We make use of digital holograms to create custom vortex beams and exploit q-plates for the conversion into CV vortex fields. We detected the polarization of the generated field

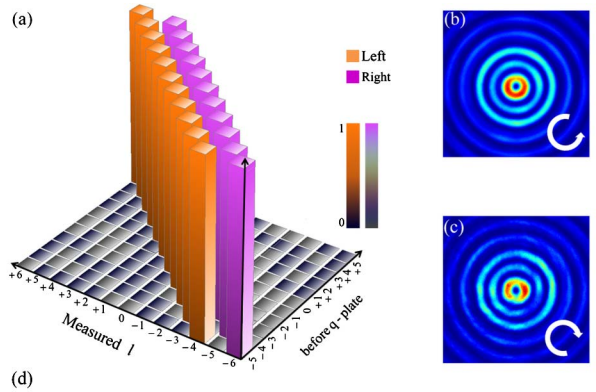

(d)

Input l:	-5	-4	-3	-2	-1	0	+1	+2	+3	+4	+5
Output l; R:	-6	-5	-4	-3	-2	-1	0	+1	+2	+3	+4
Output l; L:	-4	-3	-2	-1	0	+1	+2	+3	+4	+5	+6

Fig. 5. (a) Correlation signals for the azimuthal decomposition for both the left- (orange) and right-circular (pink) polarization components. (b) $\ell = +1$ and (c) $\ell = -1$ Bessel beams after the q-plate associated with left- and right-circular polarization components, respectively. (d) A table summarizing the transformation of the input ℓ values after the q-plate.

with the use of a PG, as well as their vortex nature by performing an azimuthal modal decomposition. In addition to their known classical applications, having the ability to simultaneously control the polarization and OAM degrees of freedom is useful in hyper-entanglement systems.

The authors acknowledge support from the U.S. National Science Foundation (NSF and ECCS-0955127) and the National Research Foundation.

References

1. Q. Zhan, Adv. Opt. Photon. **1**, 1 (2009).
2. T. G. Brown and Q. Zhan, Opt. Express **18**, 10775 (2010).
3. E. Hasman, G. Biener, A. Niv, and V. Kleiner, *Space-Variant Polarization Manipulation* (Elsevier, 2005), Vol. **47**, pp. 215–289.
4. T. G. Brown, *Unconventional Polarization States: Beam Propagation, Focusing and Imaging* (Elsevier, 2011), Vol. **56**, pp. 81–129.
5. A. M. Beckley, T. G. Brown, and M. A. Alonso, Opt. Express **18**, 10777 (2010).
6. G. Milione, H. I. Sztul, D. A. Nolan, and R. R. Alfano, Phys. Rev. Lett. **107**, 053601 (2011).
7. D. Pohl, Appl. Phys. Lett. **20**, 266 (1972).
8. Y. Mushiake, K. Matzumurra, and N. Nakajima, Proc. IEEE **60**, 1107 (1972).
9. T. Grosjean, D. Courjon, and M. Spajer, Opt. Commun **203**, 1 (2002).
10. M. Stalder and M. Schadt, Opt. Lett. **21**, 1948 (1996).
11. L. Marrucci, C. Manzo, and D. Paparo, Appl. Phys. Lett. **88**, 221102 (2006).
12. W. Han, W. Cheng, and Q. Zhan, Opt. Lett. **36**, 1605 (2011).
13. F. Cardano, E. Karimi, S. Slussarenko, L. Marrucci, C. de Lisio, and E. Santamato, Appl. Opt. **51**, C1 (2012).
14. C. Maurer, A. Jesacher, S. Fürhapter, S. Bernet, and M. Ritsch-Marte, New J. Phys. **9**, 78 (2007).
15. S. Quabis, R. Dorn, M. Eberler, O. Glöckl, and G. Leuchs, Opt. Commun. **179**, 1 (2000).
16. R. Dorn, S. Quabis, and G. Leuchs, Phys. Rev. Lett. **91**, 233901 (2003).
17. B. Jia, X. Gan, and M. Gu, Opt. Express **13**, 6821 (2005).
18. B. Hao and J. Leger, Opt. Express **15**, 3550 (2007).
19. G. M. Philip, V. Kumar, G. Milione, and N. K. Viswanathan, Opt. Lett. **37**, 2667 (2012).
20. W. Cheng, J. W. Haus, and Q. Zhan, Opt. Express **17**, 17829 (2009).
21. J. Durnin, J. J. Miceli, Jr., and J. H. Eberly, Phys. Rev. Lett. **58**, 1499 (1987).
22. R. Vasilyeu, A. Dudley, N. Khilo, and A. Forbes, Opt. Express **17**, 23389 (2009).
23. Z. Bomzon, A. Niv, G. Biener, V. Kleiner, and E. Hasman, Appl. Phys. Lett. **80**, 3685 (2002).
24. J. Tervo and J. Turunen, Opt. Commun. **192**, 13 (2001).
25. A. Niv, G. Biener, V. Kleiner, and E. Hasman, Opt. Lett. **29**, 238 (2004).
26. G. Milione, S. Evans, D. A. Nolan, and R. R. Alfano, Phys. Rev. Lett. **108**, 190401 (2012).
27. A. Flores-Pérez, J. Hernández-Hernández, R. Jáuregui, and K. Volke-Sepúlveda, Opt. Lett. **31**, 1732 (2006).
28. D. W. K. Wong and G. Chen, Appl. Opt. **47**, 602 (2008).
29. C. Lopez-Mariscal and K. Helmerson, Opt. Lett. **35**, 1215 (2010).
30. A. Dudley, R. Vasilyeu, V. Belyi, N. Khilo, P. Ropot, and A. Forbes, Opt. Commun. **285**, 5 (2012).
31. L. Marrucci, C. Manzo, and D. Paparo, Phys. Rev. Lett. **96**, 163905 (2006).
32. S. C. McEldowney, D. M. Shemo, R. A. Chipman, and P. K. Smith, Opt. Lett. **33**, 134 (2008).
33. Y. Li, J. Kim, and M. J. Escuti, Appl. Opt. **51**, 8236 (2012).
34. G. P. Crawford, J. N. Eakin, M. D. Radcliffe, A. Callan-Jones, and R. A. Pelcovits, J. Appl. Phys. **98**, 123102 (2005).
35. I. A. Litvin, A. Dudley, F. S. Roux, and A. Forbes, Opt. Express **20**, 10996 (2012).
36. D. Flamm, D. Naidoo, C. Schulze, A. Forbes, and M. Duparré, Opt. Lett. **37**, 2478 (2012).